Channel Modeling for Reflective Phased Array Type RISs in mmWave Networks

Joonas Kokkoniemi and Markku Juntti
Centre for Wireless Communications, University of Oulu
forename.surname@oulu.fi

ABSTRACT

This paper looks into channel modeling of the phased array type reconfigurable intelligent surfaces (RISs) in the millimeter Wave band (mmWave, 30–300 GHz). The RISs have been under intense investigation lately for their ability to provide control on the mmWave sparse channels. This has been shown to improve coverage and signal levels in environments where line-of-sight (LOS) paths cannot be guaranteed. In this paper, gain properties of the RISs in LOS channels are analysed with respect to frequency and size. It is shown that the RISs provide the best gain compared to LOS links at lower frequencies due to larger RIS size for the same number of antenna elements. On the other hand, high gain RISs tend to push the near field far away from the array in the low frequencies. These observations mean that different parts of the mmWave band have advantages and disadvantages when utilizing RIS assisted channels.

CCS CONCEPTS

• **Networks** → **Physical links**.

KEYWORDS

Antenna arrays, channel modeling, millimeter wave, reconfigurable intelligent surfaces

ACM Reference Format:
Joonas Kokkoniemi and Markku Juntti. 2021. Channel Modeling for Reflective Phased Array Type RISs in mmWave Networks. In *Proceedings of mmNets (mmNets '21).* ACM, New York, NY, USA, 6 pages. https://doi.org/10.1145/nnnnnnn.nnnnnnn

1 INTRODUCTION

The future communication systems look for the extreme data rates in the millimeter wave band (mmWave, 30–300 GHz). The mmWave frequencies along with the THz band (300 GHz – 10 THz) offer opportunities to increase the data rates drastically by increasing the transmission bandwidths [1, 16]. Within such a vast spectrum of frequencies, there are plenty free bands for communications offering bandwidths ranging from few gigahertz to tens of gigahertz. While potential for variety of high data rate applications, the high frequencies present some challenges in efficient utilization.

Among those are challenges with efficient hardware that generate high power and linear response with extremely high bandwidths. The high channel losses [13] and poor penetration through walls and other objects [20] render the mmWave channels sparse. The sparsity of the channels included with high gain requirements for the antennas lead to challenges in channel estimation, that is, in finding the best communication channels [11]. One very popular solution in research have been the reconfigurable intelligent surfaces (RISs), or intelligent reflective surfaces (IRSs) [7].

The RISs give control of the channel to some extent to the base stations by their ability to reflect the incoming waves toward anomalous direction by manipulating the phases of the incoming signals [7]. This means that in situations where LOS path is likely to be blocked, the RISs can steer the beam "behind the corner". By smart placement, the RISs can extend the cell coverage far beyond that of what a single fixed access point could. Thus, the RISs are acting similarly to relay stations, but with simplified hardware [8].

The RISs are often assumed to be passive in a sense that they do not receive the signals and cannot therefore adjust the phases independently [7]. The control is instead done at the base station and fed to RIS via dedicated control channel (wired or wireless). This leads to low operational and manufacturing costs, but does make the channel estimation more challenging as the base station needs to be able to optimize its own transmissions as well as the RIS phases jointly or sequentially [12]. There are multiple types of RISs, but most commonly metasurface and reflecting phased antenna array solutions are considered in the literature [7]. In this paper, we focus on the antenna array type RISs, whereas the metasurface based RISs are briefly discussed in the next section. The RISs have been shown in experimental setups to function efficiently in reflecting the signals in controlled fashion, showing that indeed great benefits can be achieved with RISs in environments where line-of-sight (LOS) paths cannot be guaranteed [9, 14, 19, 22].

In this paper, we analyse the channel gain properties compared to the LOS path gain when utilizing ideal RISs. We start with the a general channel model for RISs and derive the gain compared to LOS path in order to analyse the impact of frequency on the achievable gain. As the antenna structures may be very large at high frequencies, the near field size is also analysed with respect to size and configuration of the array. We will show that the frequency and the number of antenna elements will have great impact on the gain. Furthermore, depending on the application and environment, the shape of the RIS may also be part of the design criteria if the near field of antenna need to be avoided. In short, the gain of the RIS with fixed number of antenna elements will increase at lower frequencies due to larger antenna size, but the near field of the antenna array will increase linearly with the wavelength at the same time.

The rest of this paper has been organized as follows: A brief look into the background of the RIS modeling and channel modeling is given in Section 2, the system model and RIS models utilized in the analysis, as well as the mathematical analysis are given in

mmNets '21, October 25, 2021, New Orleans

ACM ISBN 978-x-xxxx-xxxx-x/YY/MM.
https://doi.org/10.1145/nnnnnnn.nnnnnnn

Section 3, and the numerical results are given in Section 4. Finally, the conclusions on the results in Section 5 end the paper.

2 BACKGROUND

In this section, we briefly look into the common RIS models and RIS channel models.

2.1 RIS Modeling

There are many ways to realize the RISs. Two of the most common ones considered in the literature are metasurfaces and reflective phased arrays. Metasurface reflectors are structures formed of small meta-atoms that tend to be mutually coupled and the reconfigurability of the metasurface is obtained, for instance, by geometric design and tunable materials [7].

A simpler solution from analysis point of view are the reflective phased arrays. These are essentially normal reflective antenna arrays without the base band or RF units. These structures are often considered to be fully passive besides some semi-passive structures where certain set of elements receive and help with the channel estimation [21]. The antenna array type approach allows individual phase control at each antenna. Then also the beamforming is similar to that of the regular antenna array. There is a very wide look into the RIS modelling, differences between these two different RIS types, applications, and discussion in [7]

2.2 RIS Channel Modeling

There are quite a lot of papers on channel modelling for RIS assisted links [2–7, 10, 14, 15, 18, 22]. The core link model in all of these papers is a compound channel model formed of Tx-RIS and RIS-Rx links. In the most of the above channel modeling themed works the link are assumed to be LOS. The main differences come from the handling of the beamforming. The antenna gains are important in the RIS modelling as it is possible in close range with high gain antennas to only illuminate the RIS partially [17]. This leads to decreased RIS response, but on the other hand the same occurs with the more common case when RIS captures only a small part of the incoming radiation. This latter point is analysed briefly in this paper when we show that the RIS gain decreases with distance.

The channel model utilized in this paper follows our previous work presented in [15] and it is essentially the same as in many other papers, but with optimized beamformers such that the channel gain is given in terms of the antenna gains only. This model is given in the next section with the main focus on the channel gain by RIS and the near field radii of different RIS configurations.

3 THEORETICAL RIS RESPONSE

In this section, we provide the system model, the path loss models for LOS and RIS links, as well as the near field bounds that depend on the array configurations.

3.1 System Model

The system model used in this paper is given in Fig. 1. It comprises RIS, Tx, and Rx. Those utilize phased arrays with $N_{RIS,y} \times N_{RIS,x}$ antenna elements at RIS, $N_{Tx,y} \times N_{Tx,x}$ antenna elements at Tx, and likewise $N_{Rx,y} \times N_{Rx,x}$ antenna elements at Rx. The distances between the network elements have been given as follows: $r_{\mathrm{Tx,Rx}}$ is the LOS distance from Tx to Rx, $r_{\mathrm{Tx,RIS}}$ is the distance from Tx to RIS, and $r_{\mathrm{RIS,Rx}}$ is the distance from RIS to Rx. The RIS phase Φ is not modeled in this work as we use stochastic gains based on the far field propagation models as detailed below.

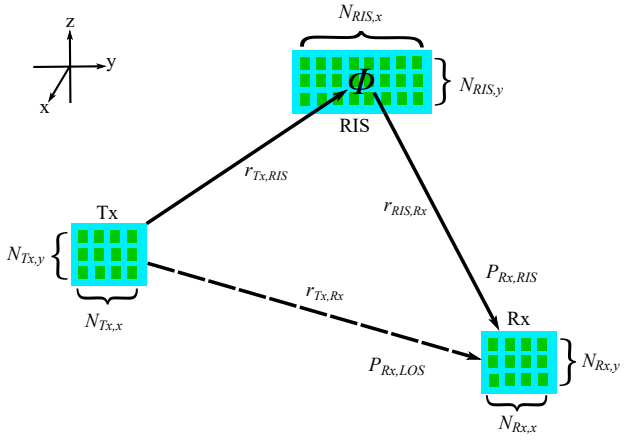

Figure 1: The system model utilized in this paper.

3.2 Path Loss Models

We use standard LOS channel model in all links. That is given in the mmWave bands by the Friis transmission equation with molecular absorption loss as [13]

$$P_{\mathrm{Rx,LOS}}(r,f) = P_{\mathrm{Tx}} G_{\mathrm{Tx}} G_{\mathrm{Rx}} \frac{c^2 e^{-\kappa_{\mathrm{a}}(f) r_{\mathrm{Tx,Rx}}}}{(4\pi r_{\mathrm{Tx,Rx}} f)^2}, \tag{1}$$

where P_{Tx} is the transmit power, $\kappa_{\mathrm{a}}(f)$ is the absorption coefficient, f is the frequency, c is the speed of light, and G_{Tx} and G_{Rx} are the Tx and Rx antenna gains, respectively.

We utilize a RIS model given in [15]. The model therein is given as

$$P_{\mathrm{Rx,RIS}} = P_{\mathrm{Tx}} G_{\mathrm{Tx}} G_{\mathrm{Rx}} G_{\mathrm{RIS}} \Gamma_{\mathrm{RIS}} \frac{e^{-\kappa_a (r_{\mathrm{Tx,RIS}} + r_{\mathrm{RIS,Rx}})} c^2 A_{\mathrm{RIS}}}{(4\pi)^3 f^2 r_{\mathrm{Tx,RIS}}^2 r_{\mathrm{RIS,Rx}}^2}, \tag{2}$$

where $r_{Tx,RIS}$ and $r_{RIS,Rx}$ are the Tx–RIS and RIS–Rx distances (see also Fig. 1), A_{RIS} is the RIS area (or capture area for the incoming energy) and G_{RIS} is the total gain of the RIS. We added in a RIS reflection coefficient, or reflection efficiency Γ_{RIS} that accounts for the non-ideal reflection power, although, it's assumed to be unit in this paper. It should be noticed that this is the maximum possible RIS channel gain. That is, the beamformers are fully optimized in the far field of the array. As a consequence, we obtain the full channel gain. In reality, the beamformers are estimated from the channel response and gain will be decreased due to any possible estimation errors at Tx, Rx, or RIS, as well as due to possible HW imperfections.

The RIS gain compared to LOS is given by division of (2) and (1) by setting the total distance in the both models to equal $r_{\mathrm{Tx,RIS}} + r_{\mathrm{RIS,Rx}}$. The resultant gain is given by

$$G_{\mathrm{RIS,LOS}} = G_{\mathrm{RIS}} A_{\mathrm{RIS}} \Gamma_{\mathrm{RIS}} \frac{(r_{\mathrm{Tx,RIS}} + r_{\mathrm{RIS,Rx}})^2}{4\pi r_{\mathrm{Tx,RIS}}^2 r_{\mathrm{RIS,Rx}}^2}. \tag{3}$$

Even with ideally reflecting RIS, we can see that the gain of the RIS compared to LOS path has certain bounds. Those include the gain and surface area of the RIS and the distance from the RIS. In real life, as well as in the ideal configuration, fully covered RIS surface with d separation distance between the individual elements, the gain and the size of the RIS are interconnected. In this paper we assume $d = \lambda/2$ separation between the antenna elements. By assuming fully covered RIS, the total area of the RIS becomes

$$A_{\text{RIS}} = [(N_x - 1)d_x + \epsilon_x] \times [(N_y - 1)d_y + \epsilon_y], \tag{4}$$

where $(N_x - 1)d_x + \epsilon_x$ and $(N_y - 1)d_y + \epsilon_y$ are the horizontal and vertical lengths of the antenna array, N_x and N_y are the number of antenna elements in horizontal and vertical directions, d_x and d_y are the corresponding antenna element separations, and ϵ_x and ϵ_y give an additional room for realistic antenna element sizes. That is, the added length in horizontal and vertical directions due to physical size of the antenna elements. Our assumptions on fully covered RIS surface hints that $\epsilon_x = \epsilon_y = d_x = d_y = d$. In any case, the total effective capture area for energy at RIS has impact on the total energy for the reflection towards the Rx. Due to limited size, the distance from the Tx or Rx to the RIS has impact on the energy captured by this area. Therefore, a finite size RIS tends to lose in gain to LOS path, but this depends on the size of RIS and distance to it as it will be shown in the numerical results. The above also gives away that the gain of the RIS is dependent on the size of the elements via their area. This in ideal setting leads to diminishing RIS size as a function of the wavelength, which leads to smaller gain with fixed number of antenna elements when moving to higher frequencies.

From above, we can show the the gain of an ideal square RIS as

$$G_{\text{RIS,LOS}} = N_{\text{RIS}}^2 d^2 \frac{(r_{\text{Tx,RIS}} + r_{\text{RIS,Rx}})^2}{4\pi r_{\text{Tx,RIS}}^2 r_{\text{RIS,Rx}}^2}, \tag{5}$$

where N is the total number of antenna elements in the RIS. The square RIS also has the smallest near field among the rectangular RIS structures. This can be a very appealing structure as the near field of the RIS can be very large with large numbers of antenna elements. This is looked into in the next section.

The received power of the RIS link is given by (2), but can also given in terms of (3) (or (5)):

$$\begin{aligned} P_{\text{Rx}}(r_{\text{tot}}) =& P_{\text{Rx,LOS}}(r_{\text{Tx,RIS}} + r_{\text{RIS,Rx}}, f)\times \\ & G_{\text{RIS,LOS}}(G_{\text{RIS}} A_{\text{RIS}}, \Gamma_{\text{RIS}}, r_{\text{Tx,RIS}} + r_{\text{RIS,Rx}}). \end{aligned} \tag{6}$$

3.3 Near Field of the RIS

It should be evident that the above models for RIS propagation are only valid in the far field of the RIS (or any other antenna in the system). However, as the future antenna systems and especially RISs can be very large to obtain the required gain levels, the near field of an antenna can be very large. Therefore, in this section we look into the near field size of an array of various phased antenna array configurations. We only focus on rectangular arrays here with different aspect ratios. Linear arrays are omitted as those are unlikely in arrays with large numbers of antenna elements.

The near field of an antenna array in general case is given by

$$R_{\text{NF}} = \frac{2D^2}{\lambda}, \tag{7}$$

where R_{NF} is the near field radius, D is the maximum dimension of the antenna, and λ is the wavelength. The maximum dimension of the antenna array is assumed to be formed by the maximum dimension of the area confined by the antenna elements as

$$D = \sqrt{[(N_x - 1)d_x + \epsilon_x]^2 + [(N_y - 1)d_y + \epsilon_y]^2}, \tag{8}$$

where the maximum distance across the antenna D herein with rectangular arrays is from corner to corner. However, in reality, the actual dimensions of the antennas depend on the type of the antenna. Here we use easily tractable mathematical arrays and the above holds for those.

Then the RIS near field radius is given by

$$r_{\text{NF}} = \frac{2}{\lambda}\left([(N_x - 1)d_x + \epsilon_x]^2 + [(N_y - 1)d_y + \epsilon_y]^2\right). \tag{9}$$

Furthermore, for ideal square RIS without the ϵ, the near field becomes

$$r_{\text{NF}} = \frac{4}{\lambda}(\sqrt{N} - 1)^2 d^2, \tag{10}$$

or $r_{\text{NF}} = 4Nd^2/\lambda$ if we assume ϵ to be equal to the antenna separation d. As mentioned above, and using the above equations, we show that the antenna configuration will have a large impact on the near field size close to large antenna arrays.

4 NUMERICAL RESULTS

In this section, we give the numerical results on impact of the RIS size at different frequencies on the achievable channel gain and the size of the near field. The frequencies herein are 30, 140, and 300 GHz, i.e., the far ends of the mmWave band, and the middle point of the D band (110 – 170 GHz).

The achievable RIS gains with optimized beamformers given by (3) are shown in Fig. 2. The gains are given for equal distances from Tx-RIS and RIS-Rx distances that are varied from 5 to 40 meters. This translates into total distances varying from 10 to 80 meters. The three different frequencies are given by solid lines for 30 GHz, dashed lines for 140 GHz, and dash-dotted lines for 300 GHz. We can see that the RIS gain obviously increases as a function of the RIS antenna elements. This directly follows from increased surface area for capturing the energy and more antenna element to bring more gain. We further see that for fixed number of antenna elements, the gain decreases when frequency increases. Although the gain remains constant across the frequencies with constant number of RIS antenna elements, the surface area of the RIS decreases with increasing frequency. This leads to the observed loss in the gain. Lastly, as we can see in (3), increasing distance decreases the RIS gain. This is due to decreased energy density at the surface of the RIS when distance is increased.

These results are inline with intuitive behavior of the RISs. The surface area of the RIS determines how much energy can be redirected at most, the number of antenna elements determine the maximum gain, and the distance determines the energy distribution across the surface. Therefore, while very potential technologies, the RISs have fundamental limits how much gain they can give at maximum. This gain is therefore important system parameter when determining the cell sizes when designing RIS assisted networks.

Figures 3–5 give the near field radii of the RIS (or any array) as a function of the antenna elements. The results are given for two

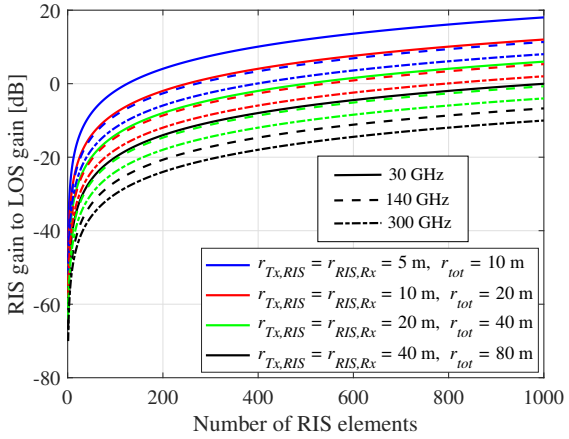

Figure 2: RIS gain as a function RIS antenna elements for various distances and three center frequencies given by solid lines for 30 GHz, dashed lines for 140 GHz, and dash-dotted lines for 300 GHz.

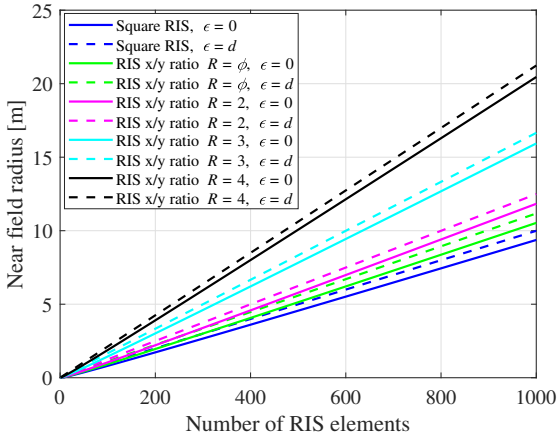

Figure 3: Near field radius of RIS for various RIS aspect ratios as a function of the number of RIS elements at 30 GHz center frequency.

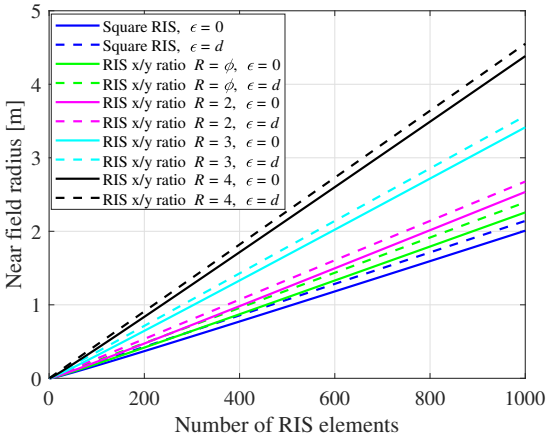

Figure 4: Near field radius of RIS for various RIS aspect ratios as a function of the number of RIS elements at 140 GHz center frequency.

options, with the ϵ parameter equal to zero or the antenna element separation distance d. Although, this only has minor impact on the near field radii due to d baing rather small. Furthermore, we give the results for various array aspect ratios. That is, the ratio R equals the difference in the horizontal length of the array against the vertical length. As an example, $R = 2$ means that there are twice the number of element in horizontal direction than in the elevation direction (although, the orientation of the antenna does not matter). For these results, we used pure mathematical ratios and the number of elements in x- and y-direction is obtained from the total number of antenna elements N with ratio R as $N_x = \sqrt{RN}$ and $N_y = \sqrt{N/R}$. To have a step between square RIS and one with aspect ratio 2/1, we used golden ratio ($\phi = (1 + \sqrt{5})/2 \approx 1.618$) as one of the ratios.

We can see in Figs. 3–5 that as expected, the near field radius increases as a function of the number of the antenna elements. Furthermore, we can see that the aspect ratio of the array has a major impact on the near field distance. This follows from increasing maximum dimension as the antenna gets smaller toward some other dimension. The maximum near field would therefore be given by a linear array. However, those are very unlikely in RIS type applications. The main observation here is related to the gain versus the frequency. When looking at Fig. 2, we can see that a RIS can theoretically exceed the LOS gain in certain setups. This is most likely with large numbers of RIS antenna elements at relatively low transmit frequency. These high gain setups, on the other hand lead to large near field close to antenna array. In certain situation, such is in indoors, the near field size has to be small enough to allow high and predictable gain. Especially in mobile applications where near field introduces fast fluctuation in the signal levels. As such, the near field radius may impose some application and environment specific limits on the RIS sizes even if the physical sizes of high frequency RISs are most likely quite modest.

Finally, Figs. 6 and 7 give the spatial distribution of the LOS power and RIS power, respectively, with 32-by-32 RIS, 16-by-16 Tx, and 4-by-4 Rx arrays at 140 GHz. We can see that the LOS link gives roughly at least 20 dB higher Rx power. If we look at Fig. 2, we see that the distances in the order of about 20 meters or less with 1024 RIS antenna elements gives in fact more gain than the LOS link. However, the increased distance via the reflected path from Tx to Rx favors the direct LOS link. This is very much expected as it is well known from literature than the RISs should be mostly beneficial in situations where the LOS link is not available.

As a final summary, the RIS gains are dependent on many factors that do not always favor their gain. Especially in realistic deployment scenarios where such massive surfaces may be difficult to realize. However, the ability steer the beams behind the corner make them very potential technologies for increasing cell sizes, decreasing the impact of blockage, serving cell edge users, creating

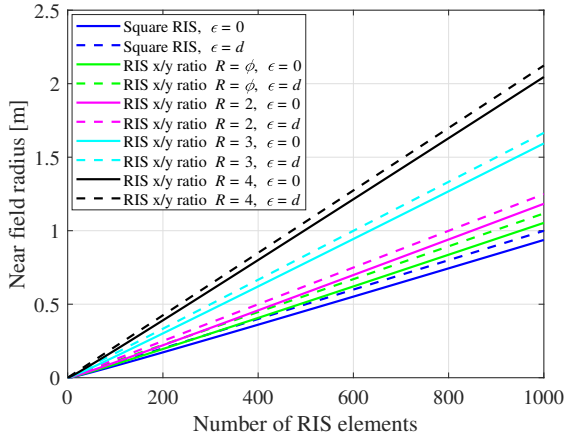

Figure 5: Near field radius of RIS for various RIS aspect ratios as a function of the number of RIS elements at 300 GHz center frequency.

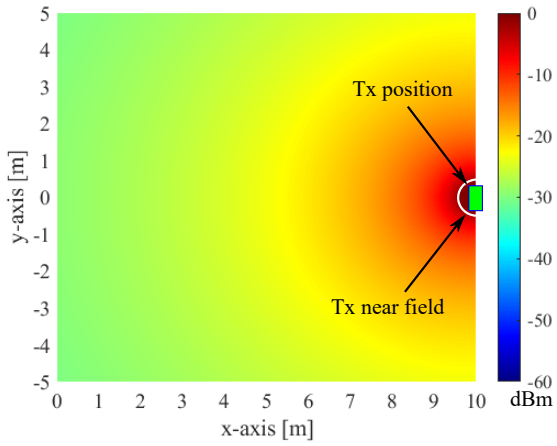

Figure 6: Received power via LOS link with 16-by-16 Tx and 4-by-4 Rx.

virtual multiple-input multiple-output (MIMO) channels, and many more applications. It thus can be expected that the RISs will be an important part of the beyond 5G networks.

5 CONCLUSION

The RISs are seen as potential technologies to increase the signal levels in environments where LOS path cannot be guaranteed. The RISs are also very potential as low cost range extenders in high frequency networks where cell sizes are small due to high path loss. In this paper, we looked into the channel modeling of RIS assisted systems. The achievable gain with respect to the LOS gain was analysed against frequency and size of the RIS. It was shown that the RIS gain decreases with frequency due to decreasing capture area for the reflected energy. However, at the same time the near field of the RIS decreases with frequency due to the same reason. This means

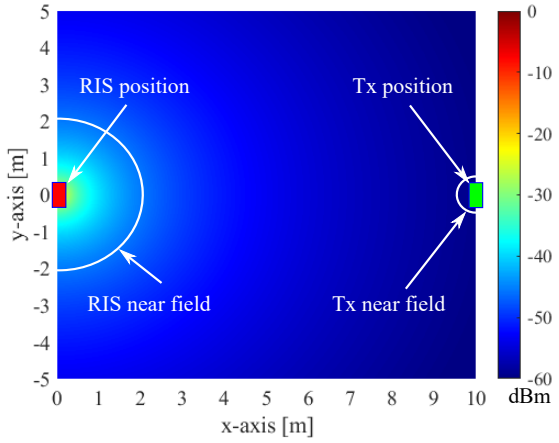

Figure 7: Received power at 140 GHz via 32-by-32 RIS with 16-by-16 Tx and 4-by-4 Rx.

that, depending on the application, there may be limitations on the size of the RIS (and therefore gain) when far field communications need to be guaranteed. Whereas, the RIS gain can exceed the LOS gain with large enough RIS size, the LOS link tends to keep the upper hand due to shorter propagation distance. The ability to control the reflection direction at RIS makes them very potential in high blockage probability scenarios, such as indoor and dense city centers. Thus, the RISs will be essential part of the future high frequency communication systems where good channels are very important.

6 ACKNOWLEDGEMENT

This work was supported by the Horizon 2020, European Union's Framework Programme for Research and Innovation, under grant agreement no. 871464 (ARIADNE). It was also supported in part by the Academy of Finland 6Genesis Flagship under grant no. 318927.

REFERENCES

[1] I. F. Akyildiz, J. M. Jornet, and C. Han. Terahertz band: Next frontier for wireless communications. *Elsevier Phys. Commun.*, 12:16–32, Sep. 2014.
[2] E. Basar and I. Yildirim. Indoor and outdoor physical channel modeling and efficient positioning for reconfigurable intelligent surfaces in mmwave bands. *arXiv: 2006.02240*, pages 1–10, 2020.
[3] A.-A. A. Boulogeorgos and A. Alexiou. Coverage analysis of reconfigurable intelligent surface assisted thz wireless systems. *IEEE Open J. Vehic. Technol.*, 2:94–110, 2021.
[4] A.-A. A. Boulogeorgos and A. Alexiou. Pathloss modeling of reconfigurable intelligent surface assisted thz wireless systems. *arXiv: 2102.08757*, pages 1–6, 2021.
[5] F. H. Danufane, M. Di Renzo, J. de Rosny, and S. Tretyakov. On the path-loss of reconfigurable intelligent surfaces: An approach based on green's theorem applied to vector fields. *arXiv: 2007.13158*, pages 1–30, 2020.
[6] M. Di Renzo, F. Habibi Danufane, X. Xi, J. de Rosny, and S. Tretyakov. Analytical modeling of the path-loss for reconfigurable intelligent surfaces – anomalous mirror or scatterer ? In *IEEE SPAWC*, pages 1–5, 2020.
[7] M. Di Renzo, A. Zappone, M. Debbah, M. S. Alouini, C. Yuen, J. de Rosny, and S. Tretyakov. Smart radio environments empowered by reconfigurable intelligent surfaces: How it works, state of research, and the road ahead. *IEEE Journal on Selected Areas in Communications*, 38(11):2450–2525, 2020.
[8] M. Di Renzo et al. Reconfigurable intelligent surfaces vs. relaying: Differences, similarities, and performance comparison. *IEEE Open J. Commun. Soc.*, 1:798–807, 2020.

[9] R. Fara, D.-T. Phan-Huy, P. Ratajczak, A. Ourir, M. Di Renzo, and J. de Rosny. Reconfigurable intelligent surface -assisted ambient backscatter communications – experimental assessment. *arXiv: 2103.08427*, pages 1–7, 2021.

[10] J. C. B. Garcia, A. Sibille, and M. Kamoun. Reconfigurable intelligent surfaces: Bridging the gap between scattering and reflection. *IEEE J. Sel. Areas Commun.*, 38(11):2538–2547, 2020.

[11] J. He, N. T. Nguyen, R. Schroeder, V. Tapio, J. Kokkoniemi, and M. Juntti. Channel estimation and hybrid architectures for ris-assisted communications. *arXiv: 2104.07115*, pages 1–6, 2021.

[12] J. He, H. Wymeersch, and M. Juntti. Channel estimation for ris-aided mmwave mimo systems via atomic norm minimization. *arXiv: 2007.08158*, pages 1–30, 2021.

[13] J. M. Jornet and I. F. Akyildiz. Channel modeling and capacity analysis for electromagnetic nanonetworks in the terahertz band. *IEEE Trans. Wireless Commun.*, 10(10):3211–3221, Oct. 2011.

[14] W. Khawaja, O. Ozdemir, Y. Yapici, F. Erden, and I. Guvenc. Coverage enhancement for nlos mmwave links using passive reflectors. *IEEE Open J. Commun. Soc.*, 1:263–281, 2020.

[15] J. Kokkoniemi and M. Juntti. Stochastic geometry based interference analysis of multiuser mmwave networks with ris. *arXiv*, pages 1–6, 2021.

[16] M. Latva-Aho and K. Leppänen, editors. *Key drivers and research challenges for 6G ubiquitous wireless intelligence*. Number 1 in 6G research visions. University of Oulu, Sep. 2019.

[17] K. Ntontin, A.-A. A. Boulogeorgos, D. Selimis, F. Lazarakis, A. Alexiou, and S. Chatzinotas. Reconfigurable intelligent surface optimal placement in millimeter-wave networks. *arXiv:2011.09949*, pages 1–14, 2020.

[18] O. Özdogan, E. Björnson, and E. G. Larsson. Intelligent reflecting surfaces: Physics, propagation, and pathloss modeling. *arXiv:1911.03359*, pages 1–5, 2019.

[19] X. Pei, H. Yin, L. Tan, L. Cao, Z. Li, K. Wang, K. Zhang, and E. Björnson. Ris-aided wireless communications: Prototyping, adaptive beamforming, and indoor/outdoor field trials. *arXiv:2103.00534*, pages 1–13, 2021.

[20] T. S. Rappaport, Y. Xing, O. Kanhere, S. Ju, A. Madanayake, S. Mandal, A. Alkhateeb, and G. C. Trichopoulos. Wireless communications and applications above 100 ghz: Opportunities and challenges for 6g and beyond. *IEEE Access*, 7:78729–78757, Jun. 2019.

[21] R. Schroeder, J. He, and M. Juntti. Channel estimation for hybrid ris aided mimo communications via atomic norm minimization. *arXiv:2106.10909*, pages 1–6, 2021.

[22] W. Tang, M. Z. Chen, X. Chen, J. Y. Dai, Y. Han, M. Di Renzo, Y. Zeng, S. Jin, Q. Cheng, and T. J. Cui. Wireless communications with reconfigurable intelligent surface: Path loss modeling and experimental measurement. *arXiv: 1911.05326*, pages 1–32, 2020.